Presented at 32nd AIAA Aerodynamic Measurement Technology and Ground Testing Conference, 13 - 17 June 2016, Washington, D. C., Paper #: AIAA 2016-3112

Disturbance and Phase Speed Measurements for Shock Tubes and Hypersonic Boundary-Layer Instability

J. S. Jewell*
U.S. Air Force Research Laboratory, Wright-Patterson AFB, OH 45433, USA
N. J. Parziale†
Stevens Institute of Technology, Hoboken, NJ 07030, USA
K.-Y. Lam‡, B. J. Hagen§, R. L. Kimmel¶
U.S. Air Force Research Laboratory, Wright-Patterson AFB, OH 45433, USA

Measurements and calculations of the phase speed of disturbances observed in a small shock tube are made, via cross-correlation of successive frames from focusing schlieren videography and double focused laser differential interferometry. The efficacy of the latter technique for measuring slender-body hypersonic boundary-layer instability wave-packets is also demonstrated. Shock tube experiments are performed to provide a known velocity input to both sensors for comparison, and measurements of phase velocity are made behind the reflected shock. Power spectral density curves from the FLDI and focusing schlieren from shock tube experiments at similar conditions are compared with each other and with pitot tube results, and reasonable agreement is found to the frequency limits of the sensors.

I. Introduction

In the study of hypersonic boundary-layer instability, recent research has focused on predicting, with numerical methods, the frequency content of disturbances that are measured over simple geometries. The motivation for these efforts is to refine the computational predictive tools when they are applied to flowfields with the most tractable and separable problems.

To facilitate the development of boundary-layer transition prediction tools, advances in experimental methods must also keep pace. Here, we focus on the application and development of two techniques: focusing schlieren deflectometry and the focused laser differential interferometer (FLDI). The focusing schlieren technique is well-known and in current use. The FLDI is here applied in a new way, set up such that two very closely spaced probe volumes permit the measurement of the phase speed or convective velocity of density disturbances in the flowfield, including in a shock tube and also for hypersonic boundary-layer instability wave-packets in a hypersonic ground-test facility. This technique will ultimately enable the measurement of both phase speed and frequency content, which should serve to support improvements in predictive capabilities.

*Research Aerospace Engineer (NRC Research Associate), AFRL/RQHF, Wright-Patterson AFB, OH 45433. jjewell@alumni.caltech.edu. AIAA Senior Member.
†Assistant Professor, Mechanical Engineering, Castle Point on Hudson, Hoboken, New Jersey, 07030. AIAA Member.
‡Research Aerospace Engineer (Spectral Energies, LLC), AFRL/RQHF, Wright-Patterson AFB, OH 45433. AIAA Member.
§Test Engineer, AFRL/RQVX, Wright-Patterson AFB, OH 45433. AIAA Student Member.
¶Principal Aerospace Engineer, AFRL/RQHF, Wright-Patterson AFB, OH 45433. AIAA Associate Fellow.

II. Focusing Schlieren Setup

A Z-type focusing schlieren[1,2] configuration is used in the present study. A high-powered LED light source with a condenser lens and a slit is used as an extended light source. The LED light source is a CXA3070 Cree X-Lamp, cool white in color, with a luminosity of 7945 Im, and is purchased from Mouser Electronics. In this configuration a heat sink is also required to conduct the heat away from the LED. In addition, a Photron SA-Z Camera with 50 mm focal length lens is used to register the schlieren images at resolutions up to 896×448 pixels with frame rates from 50,400 fps to 900,000 fps and exposure times less than 1 μs.

Figure 1 shows a schematic of the focusing schlieren imaging system deployed in the new AFRL shock tube. The optical components are comprised of the high-powered LED light source (as above), a Fresnel lens, a 360 mm $f/6.5$ focusing camera lens, and complementary source and cutoff grids. The source grid is an array of horizontal clear-and-opaque bands, which function as multiple schlieren light sources at various angles with the optical centerline. The cutoff grid is a photographic negative of the source grid and is located in a plane optically conjugate to it. The schlieren effect can be achieved with an appropriate adjustment on the cutoff grid to block a fraction of the light from reaching the image plane. With the convergence of the schlieren light beam between the source grid and the camera lens, a relatively narrow "plane of focus" can be reconstructed in the vicinity of the image plane, and refractive disturbances outside this "plane of focus" are too blurred to be registered in the image. A simple lens is placed at the image plane to focus the light into the high-speed camera. This configuration provides a depth of focus of about ±4 cm.

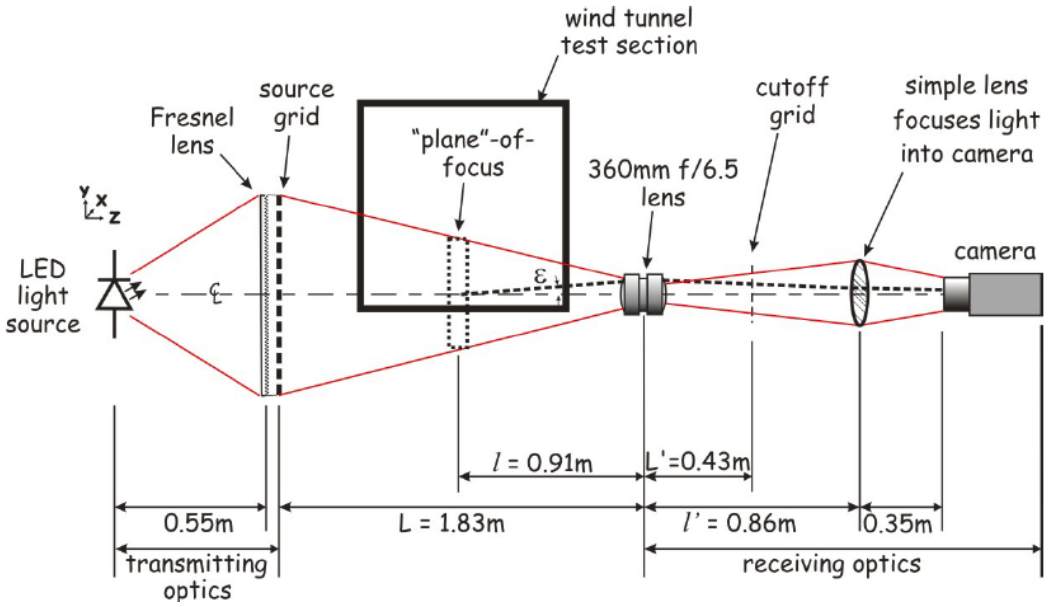

Figure 1. Schematic of focusing schlieren imaging optics.

III. Double Focused Laser Differential Interferometry (FLDI)

The FLDI[3–8] is an optical technique which permits the high-speed and non-intrusive interrogation of small-amplitude density perturbations at a small probe volume. In Smeets,[5] Figure 3 depicts the use of a Koester prism (an assembly of two identical right angle prisms) to separate a single FLDI bundle into two FLDI bundles. We refer to an FLDI bundle as the two orthogonally polarized laser beams that comprise one FLDI. In this work, we use a microscope slide placed at a prescribed angle so that approximately 1/3 of the FLDI beam is transmitted through the slide, and 2/3 of the FLDI beam is totally internally reflected and then transmitted through the slide. This setup results in a series of FLDI bundles that pass through the probe volume. The first totally internally reflected FLDI bundle has enough power to register sufficient SNR at a photodetector at the end of the beam path. The position and attitude of the microscope slide dictates the separation distance and orientation of the bundles relative to each other. A schematic of this FLDI setup

is presented as Figure 2. In the shock tube experiments described in Section IV, the beam separation is 1620 µm for the double FLDI setup.

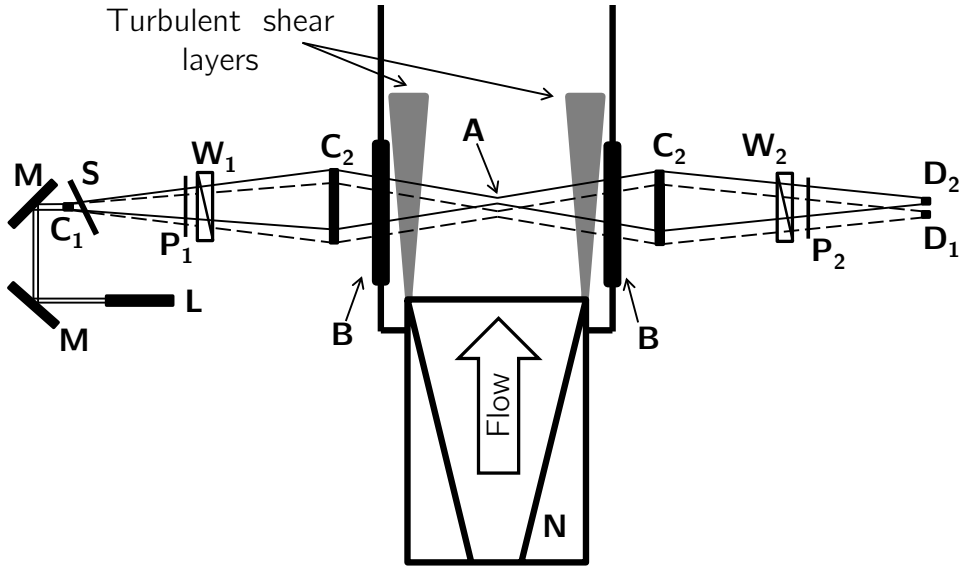

Figure 2. Annotated schematic of the FLDI. L, Laser; M, mirror; C_1, 10 mm focal length lens; C_2, 300 mm focal length lens; P, polarizer; W, Wollaston prism (2 arc minutes); B, BK7 window; A, probe volume; D_1 and D_2, photodetectors; S, Microscope slide, N, nozzle. Solid and dashed lines are used to denote the separated FLDI bundles.

A similar setup has also been used in the Caltech T5 Hypervelocity Reflected Shock Tunnel[9] to measure disturbances in the boundary layer on a slender five degree half-angle sharp cone in one case, which was part of the test campaign described in Parziale[10] and Jewell.[11] In this case, presented in Section V, the two FLDI bundles are displaced approximately 1000 µm from each other.

IV. Shock Tube Focusing Schlieren and FLDI Results

Single and double FLDI experiments, to compare FLDI-measured velocities with flowfield features of known velocity (such as shock waves) as well as to measure phase speeds or convective velocities of disturbances with unknown velocities (such as disturbances that may be present in the regions after the initial or reflected shock), are performed in a stainless steel shock tube at the U.S. Air Force Research Laboratory (AFRL) at Wright-Patterson Air Force Base, Ohio. The shock tube is comprised of a 4 m driven section and a 1 m driver section, with an inner diameter of 9.72 cm, as shown in rendered form in Figure 3 and schematically in Figure 4. A pair of flat fused-silica windows is mounted on the wall of the shock tube at a location of 82 cm from the driven section's end wall, to allow for optical imaging of the flow field. Three Kulite pressure transducers are installed in the wall over the last 1 m of the driven section to measure the traveling time of the shock front, and another Kulite pressure transducer is used as a flush-mounted pitot probe mounted in a cylindrical tube, and positioned on the shock tube centerline near the center of the window through which the optical methods gain access. The FLDI sensor is positioned directly in front of the pitot probe for FLDI experiments, and the camera is centered at this same location for the focusing schlieren experiments.

Prior to the experiment, both driver and driven sections are pumped down by a vacuum pump. In the present study, the driven section is filled up to 88, 123, and 142 Torr of air in separate double FLDI experiments, and 148, 292, and 446 Torr of air for matched pairs of experiments with single FLDI and focusing schlieren. This is followed by pressurizing the driver section with air until the breakage of the diaphragm. Once the diaphragm breaks, a shock wave is formed and travels along the driven section at (for example, for the 123 Torr condition) $M_s = 1.6$ and $V_s \approx 519$ m/s. The pressure behind the incident shock wave increases by a factor of 2.8 nearly instantaneously, and the shock-heated gas lags behind the shock wave at a velocity of ~264 m/s. The shock wave then arrives at the end wall of the driven section and is reflected, causing another step change in temperature and pressure behind the reflected shock wave.

Figure 5 presents an example of the pressure signals acquired during a typical shock tube run.

Figure 3. AFRL shock tube rendering.

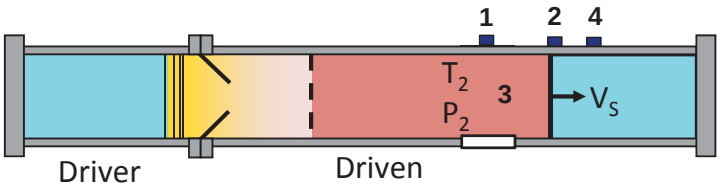

Figure 4. AFRL shock tube schematic, with locations indicated for wall pressure transducers 1, 2, and 4, and pitot transducer 3.

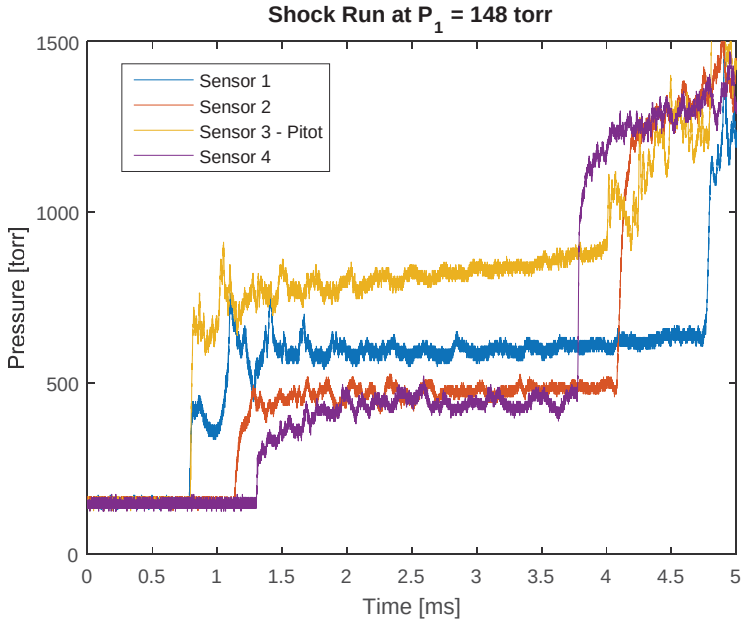

Figure 5. Pressure data, including pitot, from a typical shock tube experiment. The transducer locations are indicated in Figure 3.

Figure 6 shows a schlieren image of the shock-heated gas moving towards the driven section's end wall (from right to left). It appears that the flow is not perfectly uniform at this location, which might be attributed to the edge effect from the flat windows. Note that the width of the reflected shock front is supposed to be rather thin (within a few mean free paths). However, the measured shock front appears fairly thick or multi-valued, again possibly due to the effect of the flat windows, though the focusing schlieren should ensure that the signal received is disproportionately from the centerline.

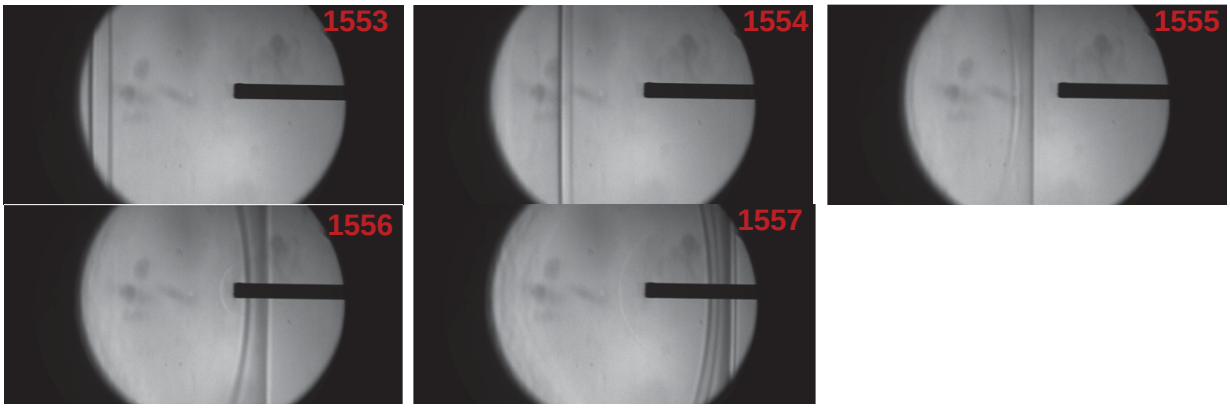

Figure 6. Focusing schlieren images from five successive frames of incident shock propagation for a shock tube experiment. The pitot probe is visible as a shadow.

Turbulent structures are observed in the frames subsequent to the shock passage. For analysis at high frame rate (900,000 fps with shutter time 1/1,260,000 s), a small window of 128 by 56 pixels is selected directly in front of the pitot probe, from which a small 4 by 4 subset, as depicted in Figure 7, is selected for frequency and velocity analysis. The shock speed is also directly measured by correlating these two signals. For the 148 Torr case, the incident shock speed was measured at 710.8 m/s with the focusing schlieren (the value from the transducers was 769 m/s); for the 292 Torr case, the incident shock speed was measured at 627.2 m/s with the focusing schlieren (the value from the transducers was 612 m/s); and for the 446 Torr case, the incident shock speed was measured at 561.2 m/s with the focusing schlieren (the value from the transducers was 557 m/s). The focusing-schlieren derived shock speed varies by less than 7% in all cases from that measured using the pressure transducers (e.g. in Figure 5).

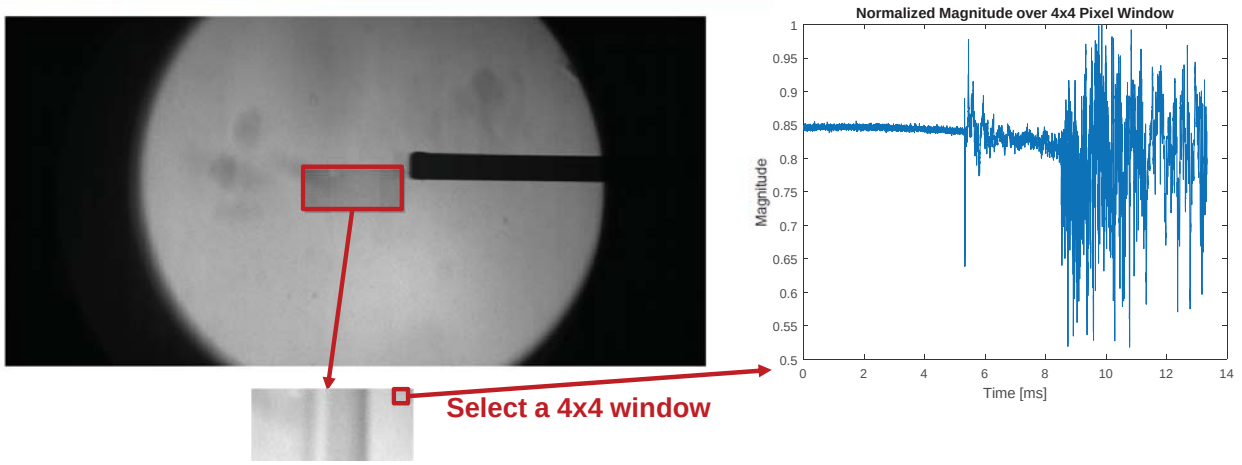

Figure 7. A small window of 128 by 56 pixels is selected directly in front of the pitot probe, from which a small 4 by 4 subset is selected for frequency analysis. For cross-correlation, a second 4 by 4 window (not pictured) on the far left side of this small window is selected.

A spectrogram (in arbitrary units calculated with the initial fill density) of a similar shock tube experiment, derived from a single-beam FLDI signal recorded at 20 MHz, is presented in Figure 8. The incident shock wave passes at the 0 ms point, with broadband disturbance across the entire spectrum, while frequency content after the shock is mostly limited to the range less than 1000 kHz. At 3.2 ms the reflected shock

passes again across the sensitive region, with a similar but stronger broadband signal due to the increased density, and again followed by a region of primarily disturbances in the relatively low frequency range.

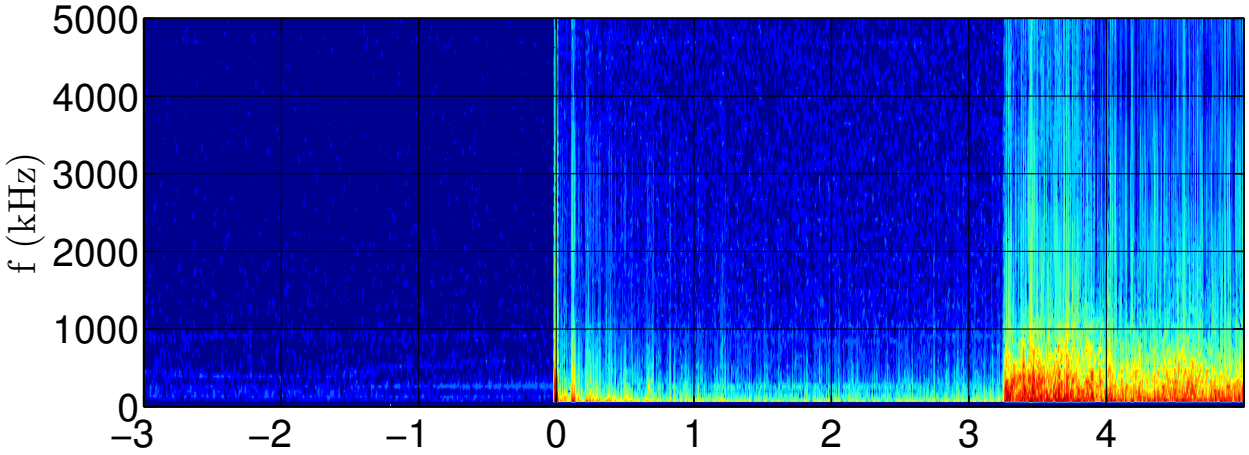

Figure 8. FLDI spectrogram for a shock tube experiment, arbitrary units calculated with the initial fill density. The time scale is in milliseconds.

A cross-correlation of double FLDI signals was performed for several shock tube conditions. The post-reflected shock region (similar to that observed after 3.2 ms in Figure 8, but in double FLDI experiments) contained coherent structures aligned along the long axis of the shock tube, which is the necessary orientation for FLDI sensitivity. An example of these cross-correlated results, which are used together with the beam separation to calculate phase velocities across the entire signal with several different window sizes, are presented in Figure 9 compared with a pitot signal recorded simultaneously just downstream of the FLDI to indicate the reflected shock region, from about 2 to 4 ms. A phase or disturbance velocity of about -400 m/s is observed in this region for all window sizes; however, outside of this region no coherent structures strong enough to consistently cross-correlate were detected. It is possible that structures also exist in the other regions, but not in the sensitive orientation for the FLDI, or that the signal to noise ratio is not strong enough in the other regions. However, significant improvements in signal to noise ratio should be possible with the use of specialized optics for splitting the sensor bundles, rather than a glass slide.

Figure 10 presents a comparison of single FLDI and focusing schlieren signals and power spectral density. These results were obtained from two separate experiments performed at nearly the same conditions (estimated variability was 5%). Good agreement is observed in PSD rolloff between the two measurements at 148 Torr out to the limit of the focusing schlieren's Nyquist frequency in this case, and also in the other two pairs experiments, at 292 and 446 Torr (not pictured).

V. Double FLDI Boundary Layer Results

In Figure 11, we present the short time Fourier transform of the FLDI response for the upstream bundle (registered by D_1 in Figure 2). In that signal, we observe narrow-band response that is consistent with the "Mack"[12–14] or second mode. An example of narrow-band response (NBR) is indicated in Figure 11, as well as an example of broad-band response (BBR).

The narrow-band response, marked by NBR, at approximately 1800 µs in Figure 11 is of interest. A 24 µs window about this wavepacket is presented as a spectrogram in Figure 12-left. Moreover, we present the upstream and downstream responses of the double FLDI system as Figure 12-top. The traces looks very much the same, except they are slightly displaced in time. The local extrema are found with signal processing in MATLAB. The difference in time, or *Delay*, is then found for the peaks (unfilled circles) and troughs (filled circles) as reported in Figure 12-bottom. Because the delay and the length (≈1000 µm) between the detectors is known, a velocity scale can be found; this velocity scale is the local phase speed. Upon inspecting Figure 12-bottom, the average delay is approximately 0.4 µs, so the local phase speed is approximately 2.5 km/s. This is approximately 80% of the edge velocity.

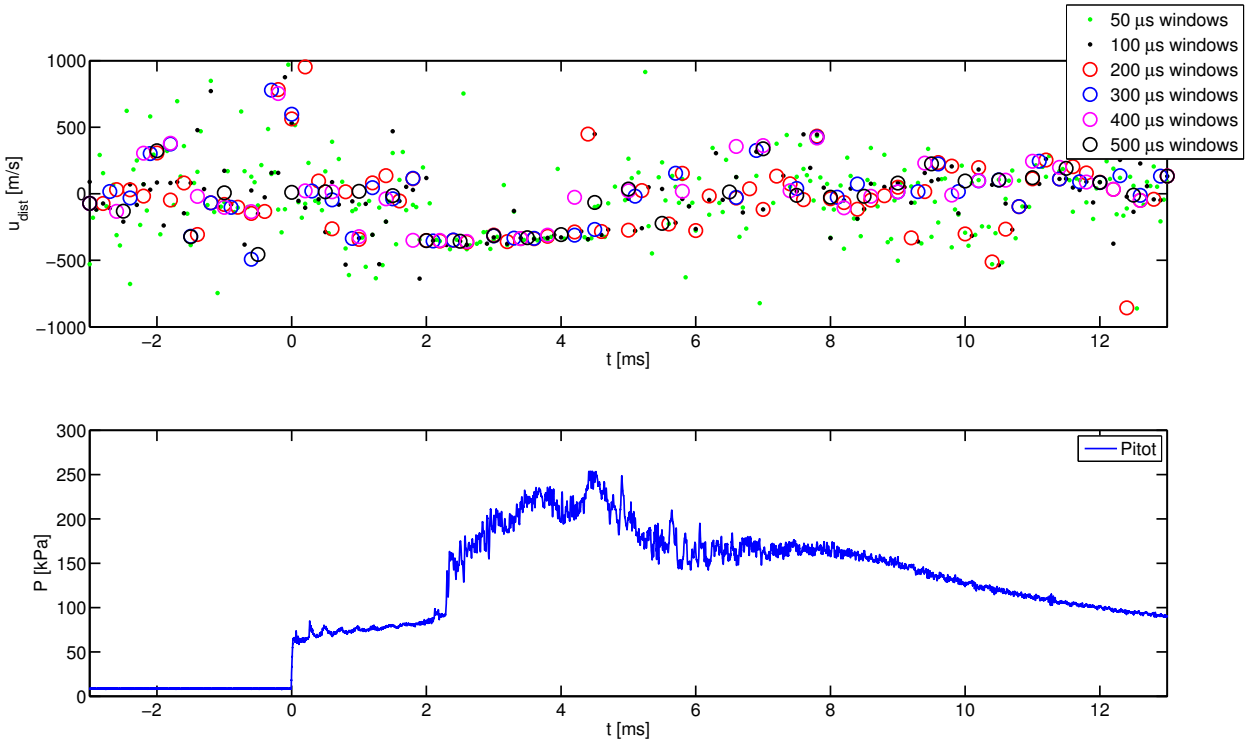

Figure 9. Cross-correlation of double FLDI signals for one shock tube experiment, compared with simultaneous pitot measurements recorded just downstream. A phase velocity of about -400 m/s is observed in the reflected shock region (from about 2 to 4 ms) for all window sizes; however, outside of this region no coherent structures strong enough to reliably cross-correlate were detected, as the random distribution of cross-correlated phase speeds indicate.

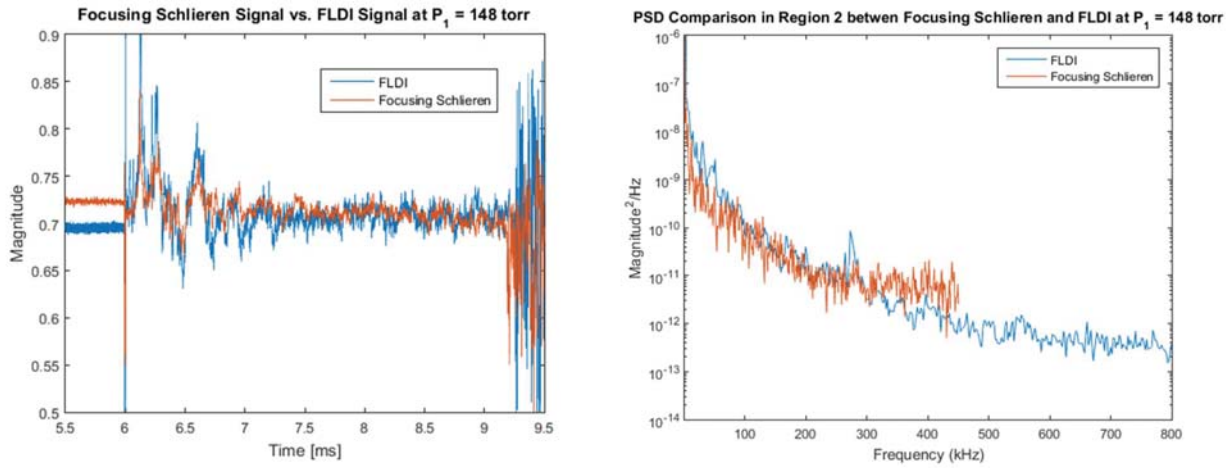

Figure 10. FLDI and focusing schlieren signals (left) and power spectral density (right) compared. Good agreement is observed in PSD rolloff between the two measurements out to the limit of the focusing schlieren's Nyquist frequency.

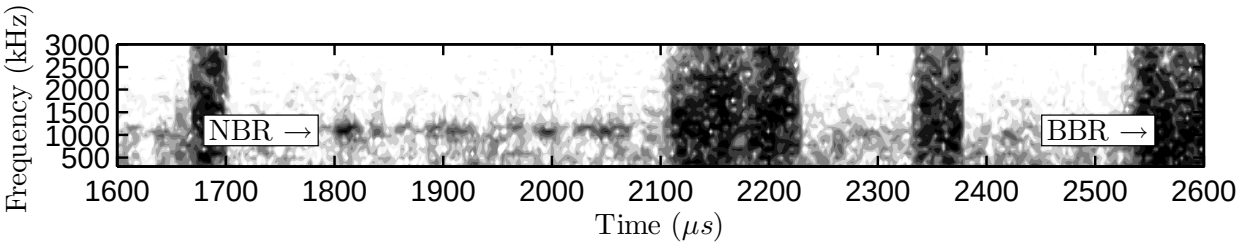

Figure 11. Arbitrary logarithmic units of change in density, the spectrum is estimated by the short time Fourier transform. Darker shading indicates larger amplitude. BBR is broadband response, NBR is narrowband response.

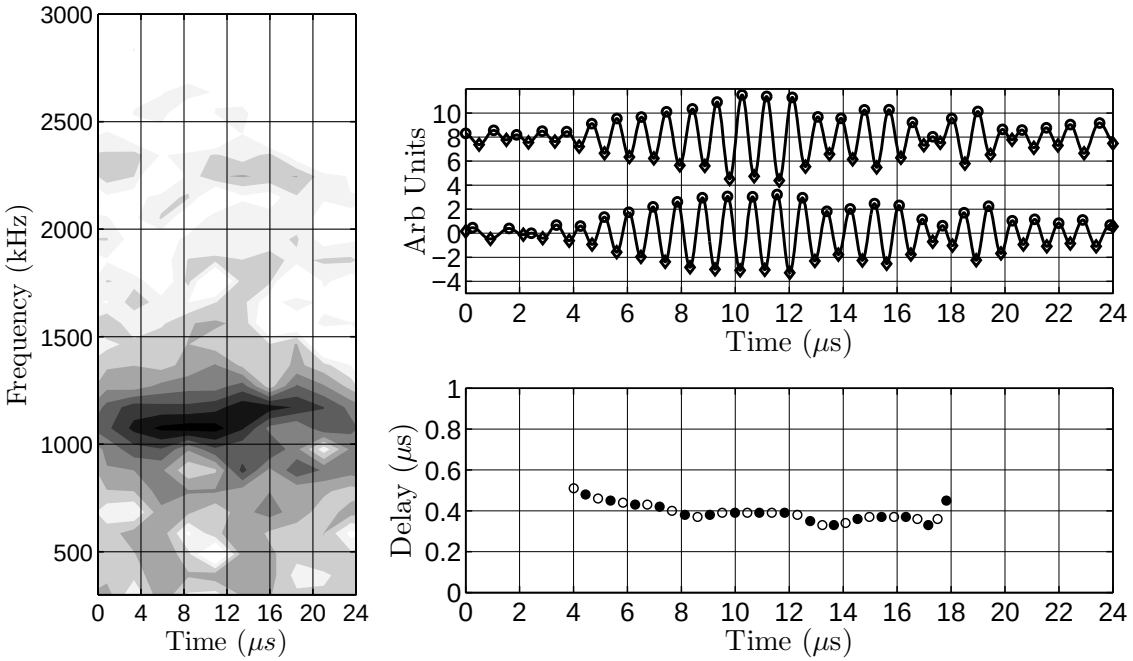

Figure 12. *Left:* **Zoomed in spectrogram around 24 µs of the narrow-band disturbance indicated at approximately 1800 µs by NBR in Figure 11.** *Top:* **Upstream and downstream FLDI responses recorded by detectors D_1 and D_2 in Figure 2.** *Bottom:* **The delay in µs of the upstream and downstream response for the peaks (unfilled circles) and troughs (filled circles).**

Trends in the structure of Figure 12-bottom are apparent. The phase speed appears to vary depending on the location within a wave-packet and the stage at which it passes through the FLDI probe volumes, but further investigation will be required to confirm this effect.

Table 1. Summary of reservoir and edge conditions for shot 2821 in 50% CO_2, 50% air by mass. For further details on this condition see Jewell and Shepherd.[15]

Shot	h_{res} (MJ/kg)	P_{res} (MPa)	U_e (m/s)	P_e (kPa)	T_e (K)	Tv_e (K)	ρ_e (kg/m^3)	M_e (-)	unit Re_e (1/m)
2821	6.70	42.5	3063	37.2	1362	1362	0.110	4.46	7.23×10^6

VI. Future Work

Further work with the dual-beam FLDI apparatus will be pursued as part of a series of experiments on a slender 7-degree half-angle cone of variable bluntness, similar to the work performed with an 8-degree cone by Stetson[16] and recently analyzed by Jewell and Kimmel.[17] For this test campaign, the distance between the FLDI bundles will be more precisely determined and a error analysis of phase-speed measurement will be made, together with examination of possibly variable phase speed within individual wave packets.

Furthermore, additional shock tube results will be acquired to ascertain the performance of the double FLDI sensor over a wider range of conditions. Complementary computations of the shock tube flowfield, as well as the flowfield and stability properties of the 7-degree cone experiments, are also planned.

Acknowledgments

This research was performed while J. S. Jewell held a National Research Council Research Associateship Award at the Air Force Research Laboratory. The authors thank M. P. Borg of AFRL for his assistance with operating the data acquisition system for the work reported in Section IV. J. E. Shepherd of the California Institute of Technology served as the PI for the preliminary data reported in Sections III and V.

References

[1]Settles, G. S., *Schlieren and Shadowgraph Techniques*, Springer-Verlag Berlin Heidelberg, First ed., 2001.

[2]Weinstein, L. M., "Large-Field High-Brightness Focusing Schlieren System," *AIAA Journal*, Vol. 31, No. 7, 1993, pp. 1250–1255. doi: 10.2514/3.11760.

[3]Smeets, G., "Laser Interferometer for High Sensitivity Measurements on Transient Phase Objects," *IEEE Transactions on Aerospace and Electronic Systems*, Vol. AES-8, No. 2, 1972, pp. 186–190. doi: 10.1109/TAES.1972.309488.

[4]Smeets, G., "Laser-Interferometer mit grossen, fokussierten Lichtbündeln für lokale Messungen," ISL - N 11/73, 1973.

[5]Smeets, G., "Verwendung eines Laser-Differentialinterferometers zur Bestimmung lokaler Schwankungsgrössen sowie des mittleren Dichteprofils in cinem turbulenten Freistrahl," ISL - N 20/74, 1974.

[6]Parziale, N. J., Shepherd, J. E., and Hornung, H. G., "Differential Interferometric Measurement of Instability in a Hypervelocity Boundary Layer," *AIAA Journal*, Vol. 51, No. 3, 2013, pp. 750–754. doi: 10.2514/1.J052013.

[7]Parziale, N. J., Shepherd, J. E., and Hornung, H. G., "Free-stream density perturbations in a reflected-shock tunnel," *Experiments in Fluids*, Vol. 55, No. 2, 2014, pp. 1–10. doi: 10.1007/s00348-014-1665-0.

[8]Fulghum, M. R., *Turbulence measurements in high-speed wind tunnels using focusing laser differential interferometry*, Ph.D. thesis, The Pennsylvania State University, 2014.

[9]Hornung, H. G., "Experimental Hypervelocity Flow Simulation, Needs, Achievements and Limitations," *Proceedings of the First Pacific International Conference on Aero Sc. and Tech.*, Taiwan, 1993.

[10]Parziale, N. J., *Slender-Body Hypervelocity Boundary-Layer Instability*, Ph.D. thesis, California Institute of Technology, 2013.

[11]Jewell, J. S., *Boundary-Layer Transition on a Slender Cone in Hypervelocity Flow with Real Gas Effects*, Ph.D. thesis, California Institute of Technology, Pasadena, CA, 2014.

[12]Mack, L. M., "Linear Stability Theory and the Problem of Supersonic Boundary-layer Transition," *AIAA Journal*, Vol. 13, No. 3, 1975, pp. 278–289. doi: 10.2514/3.49693.

[13]Mack, L. M., "Boundary-Layer Linear Stability Theory," *AGARD Rep 709*, Special Course on Stability Transitional Laminar Flows 1984.

[14]Mack, L. M., "Stability of Axisymmetric Boundary layers on Sharp Cones at Hypersonic Mach Numbers," *Proceedings of 19th AIAA Fluid Dynamics, Plasma Dynamics and Lasers Conference*, AIAA-1987-1413, Honolulu, Hawaii, 1987. doi: 10.2514/6.1987-1413.

[15]Jewell, J. S. and Shepherd, J. E., "T5 Conditions Report: Shots 2526–2823," Tech. rep., California Institute of Technology, Pasadena, CA, June 2014, GALCIT Report FM2014.002.

[16]Stetson, K. F., "Nosetip Bluntness Effects on Cone Frustum Boundary Layer Transition in Hypersonic Flow," *Proceedings of the AlAA 16th Fluid and Plasma Dynamics Conference*, AIAA-83-1763, Danvers, Massachusetts, 1983. doi: 10.2514/6.1983-1763.

[17]Jewell, J. S. and Kimmel, R. L., "Boundary Layer Stability Analysis for Stetsons Mach 6 Blunt Cone Experiments," *AIAA SciTech 2016*, AIAA-2016-0598, 2016. doi: 10.2514/6.2016-0598.